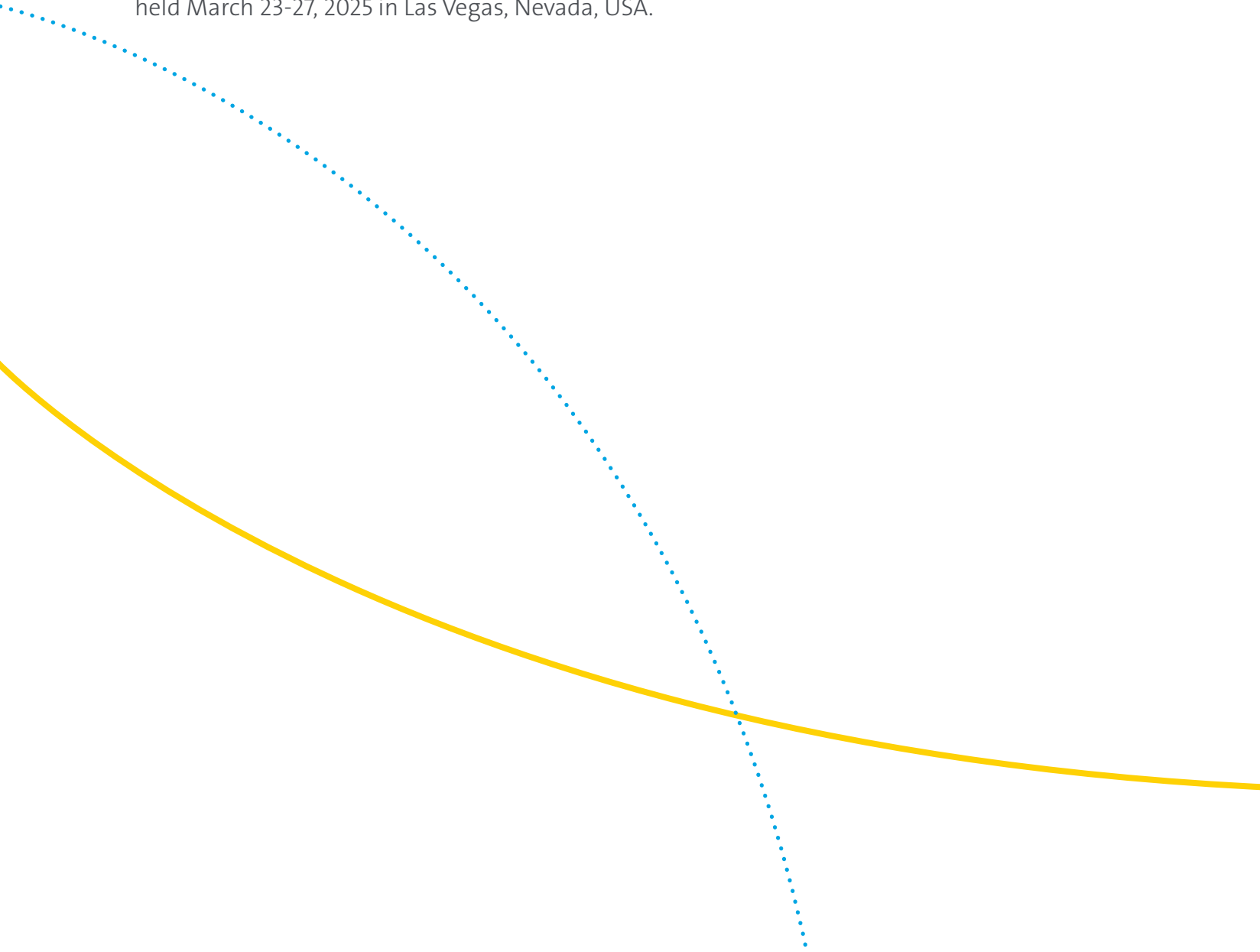# Oxy-fuel combustion:
Impact of hydrogen combustion on aluminum melt quality in secondary melting processes

Pooyan Kheirkhah, Valmiro Sa, Anandkumar Makwana

Abstract

Using fuels that produce low greenhouse gas emissions in heavy industries is a promising method to reduce their carbon footprint, and hence an effective method in combating global warming. Hydrocarbon-based fuels are commonly used in metal melting furnaces utilizing air- or oxy-fuel burners. It is critical to understand the effect of using low-carbon fuels (hydrogen) on the melting process and the quality or properties of the melt. In this study, experiments are conducted using a test furnace equipped with burner technology for various fuel combinations. This test furnace allows for a more focused study to identify how a change in the furnace atmosphere impacts the aluminum melt and dross formation.

X-ray diffraction (XRD) and Scanning Electron Microscopy/Energy Dispersive X-ray Spectroscopy (SEM/EDS) analyses of the slag layer and the core metal were conducted to evaluate the effect of using oxy-hydrogen combustion on the melting process. The results were compared against baseline oxy-natural gas combustion, under similar furnace heat-up ramp rate and melting period. The results show that elevated water vapor concentration and the absence of carbon dioxide in the furnace atmosphere when using hydrogen as fuel didn't impact the total oxides formation significantly during the melting process as compared to natural gas combustion. XRD analysis of the slag layer shows similar oxides in the melt from both hydrogen and natural gas combustion, while the hydrogen combustion melt showed presence of Al_2O_3.

1.0 Introduction

Aluminum production through secondary melting using recycled scrap requires a fraction (5%–10%) of the energy required to produce aluminum from its natural ore[1]. Combustion of conventional fuels (e.g., natural gas (NG)) in a reverberatory or a rotary furnace is a major source of carbon dioxide (CO_2) emissions.

Low-carbon intensity hydrogen (H_2) is being considered a key fuel in decarbonizing these furnaces. The use of hydrogen will affect the flame properties (e.g., no soot formation due to the absence of carbon in the fuel), emissions (NO_X), and furnace atmosphere, as no CO_2 is produced from hydrogen combustion. The change in flame properties and the impact on the thermal efficiency and NO_X emissions can be addressed through specific burner designs. The change in furnace atmosphere due to the switch from NG to H_2 can potentially impact aluminum melt and dross quality and is an area of active study. [2–4]

Application of oxy-fuel burners in secondary melting furnaces have demonstrated significant fuel efficiency gains as compared to cold air-fuel burners, reducing the NG fuel usage by up to 45%[5]. In gas fired furnaces, the use of oxy-hydrogen burners has the potential to reduce the operational carbon footprint of melting furnaces. The use of oxygen helps to optimize the amount of fuel used (per lb of material produced) and therefore, the total cost of the fuel. However, it is important to ensure that the use of oxy-hydrogen burners will not impact the process or the furnace.

The atmosphere resulting from the combustion of hydrogen with oxygen has a higher concentration of superheated water vapor (H_2O) as compared to oxy-natural gas or air-H_2 burners. The high concentration of water vapor can increase the amount of dissolved hydrogen in the liquid aluminum[6] and this undesirable dissolved hydrogen can be removed during a degassing process after melting[7]. Additionally, the furnace gases react with the molten melt forming oxides (dross) and leads to melt losses, affecting the furnace yield. More recently, studies have reported different behaviors on total dross formation by use of H_2 fuel. Piquard et al.[4] reported a similar amount of total dross formed by use of H_2-O_2 and NG-O_2 flame for P1020 and 5182 alloys (5 Mg wt. %). A study by M. Syvertsen et al.[3] found that metal oxidation with high Mg (4.7 wt. %) alloy increased with the use of H_2 as a fuel. A recent study has demonstrated that high furnace H_2O concentration (above 69 vol. %) resulted in lower dross formation as compared to dry and mid-furnace H_2O concentration (up to 32 vol. %) for AlMg5 (4.93 Mg wt. %) and EN AW-7050 (2.21 Mg wt. %) alloys because of formation of a protective MgO surface layer[2]. These differences in findings highlight a need to look at how the dross formation mechanism is impacted by switching to H_2 fuel.

In this study, the effect of changes in the furnace atmosphere, by switching the fuel from natural gas to hydrogen, on melting characteristics of aluminum alloy 6061 is investigated. Subsequent effects of such a fuel change on the amount of dross formed and the composition of the oxides formed in the dross layer is studied using X-ray diffraction (XRD) and Scanning Electron Microscopy/Energy Dispersive X-ray Spectroscopy (SEM/EDS).

2.0 Test furnace and experiment protocol

2.1 Test furnace

Air Products' US Advanced Clean Energy Laboratory has a refractory-lined custom-designed box furnace for conducting batch melting experiments **(Fig. 1)**. The furnace provides flexibility to replace the burner type and is instrumented with a gas analyzer to measure flue and furnace gas composition (CO_2, O_2, CO, NO_X), and thermocouples to monitor the temperature of the furnace atmosphere, refractory walls, furnace crown, and the flue gas. An optical window allows a view of the melting process. Crucibles of different shape/sizes pre-filled with charge material can be placed on the furnace floor using an accessible furnace door.

Figure 1 – Test furnace.
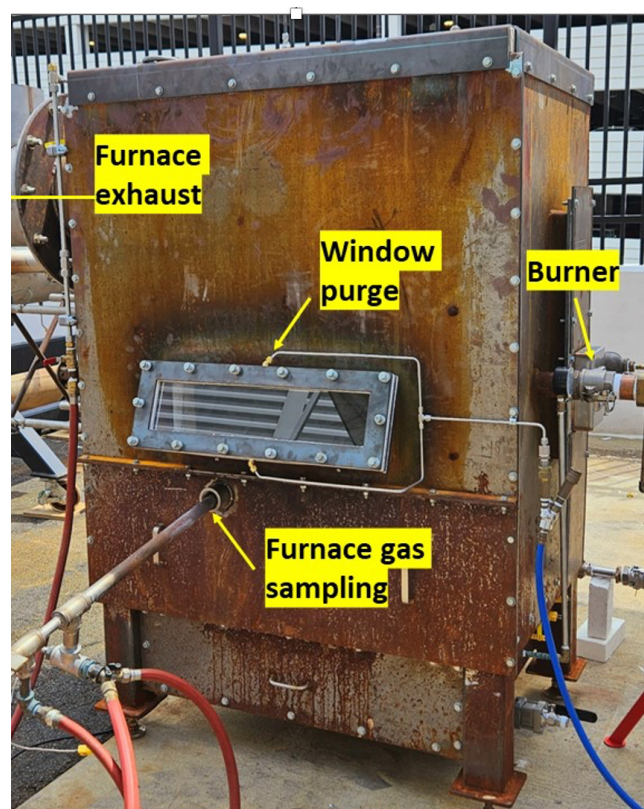
2.2 Burner

The burner used for this study is an oxy-fuel burner, operated with NG and H_2 fuels. The burner design is used only for testing in this furnace so as to produce short flames and help generate specific furnace atmosphere conditions (gas composition and temperature) similar to what is expected in an actual reverb or rotary furnace. The oxygen and fuel flow rates are controlled with instrumented flow skids.

Air Products has commercialized a smart Transient Heating Burner technology[8] that can be used in reverb furnaces. These burners are fuel-flexible (can operate with NG, H_2 or blends), and produce lower emissions (NO_X) as compared to conventional oxy-fuel burners.

2.3 Experimental plan

Melt quality and oxide formation depend on several factors, including the material being melted (% Mg in the material, type of alloy), maximum and average furnace and melt temperature, time duration, temperature-time history of the melting cycle, melt surface area exposed to the furnace atmosphere, flame type (type of burner and fuel or oxidizers used), and furnace atmosphere. In this study, all of these potential parameters that can impact the melt were kept similar across different experiments with the exception of the fuel type to investigate how a change in fuel composition can impact melt and slag/dross properties.
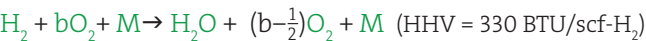
Two experiments were performed, each using 100% NG and 100% H_2 fuel with oxygen (purity: >98%) as an oxidizer. Burner firing rate and excess oxidizer (5–7%) were kept the same for both experiments. The excess oxygen is needed for furnace safety and the flow rate of oxygen is controlled to achieve similar O_2 concentrations inside the furnace.

The combustion of methane (main component in natural gas) and hydrogen with excess oxygen is represented with the following one-step global reactions:

Equation 1

$$CH_4 + aO_2 + M \rightarrow CO_2 + 2H_2O + (a-2)O_2 + M \quad (HHV = 1050 \text{ BTU/scf-}CH_4)$$

Equation 2
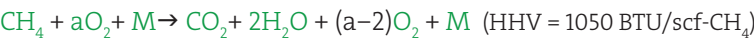
$$H_2 + bO_2 + M \rightarrow H_2O + (b-\tfrac{1}{2})O_2 + M \quad (HHV = 330 \text{ BTU/scf-}H_2)$$

where a and b are mole or standard volume ratios of oxygen to fuel, where a=2 and b=0.5 will result in stoichiometric oxygen for complete fuel combustion. An oxidizer-to-fuel flow ratio higher than the theoretical amount will carry the excess oxygen needed to ensure complete combustion of the fuel.

The combustion thermal power and the concentration of O_2, H_2O, and CO_2 in the furnace gases are summarized in **Table 1**.

Table 1 – Conditions inside the test furnace during melting operation.

| Fuel/Oxidizer		NG/O_2	H_2/O_2
Thermal Power	MMBTU/ hr	0.4	0.4
Excess O_2 from the burner	%	5–7 ($\Phi = 0.94$)	5–7
[O_2] wet basis	Vol %	2.5–4.0	2.5–4.0
[H_2O] wet basis	Vol %	60–65	95–97
[CO_2] wet basis	Vol %	30–33	0

2.4 Experimental protocol

Before experiment begins: The charge metal consists of aluminum alloy 6061 (material composition shown in **Table 2**) cubes (2"x2"x1") placed inside two separate crucibles of stainless steel and ceramic construction. These crucibles, pre-filled with loads, are placed in the test furnace before the start of the experiment. For each crucible material type, dimensions of the crucibles are the same for both experiments.

Figure 2 shows the two crucibles inside the test furnace. This figure also shows a representative flame above the two crucibles. Both crucibles are equipped with thermocouples at different depths to monitor the gas and the melt temperatures. The weight of the crucibles and aluminum charge is measured prior to and after the experiment.

Table 2 – Aluminum alloy composition

| Element	Al	Mg	Mn	Cr	Fe	Si	Ti	Cu	Zn and Zr
wt. %	95.1–98.2	0.8–1.2	0–0.15	0.05	0–0.7	0.4–0.8	0–0.15	0.05–0.4	0–0.25

Figure 2 – Location and arrangement of crucibles inside the furnace
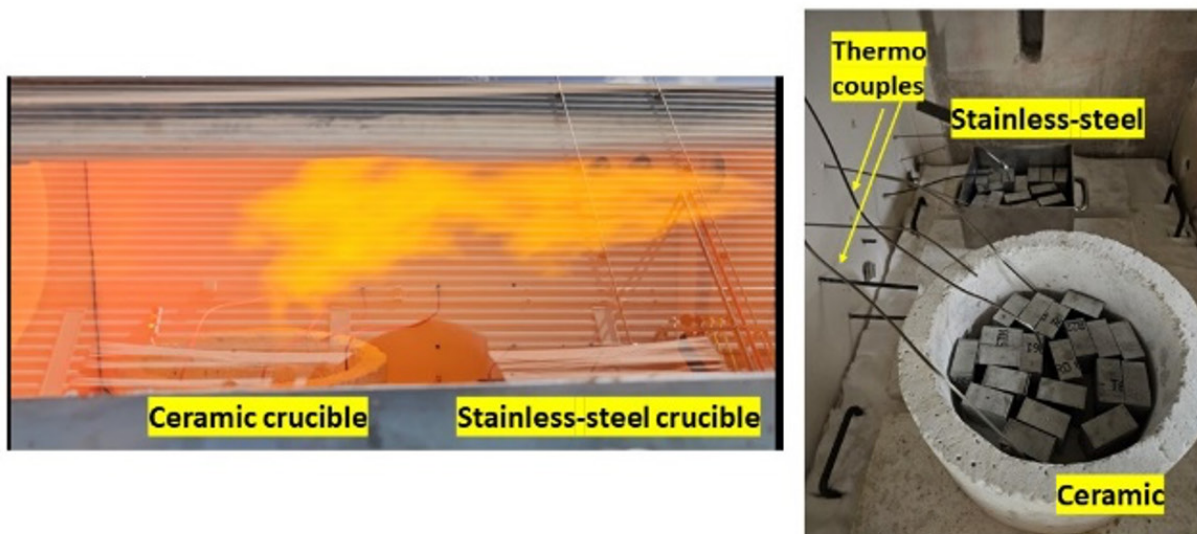
Experiment: The burner is lighted and ramped to 0.4 MMBtu/hr firing rate. Furnace gas and flue gas composition are monitored throughout the experiment. **Figure 3** shows a comparison of average furnace, exhaust flue gas, and 'inside crucible' temperatures of the NG-O_2 and H_2-O_2 experiments.

The temperature plots in **Figure 3** show a similar temperature-time history for the two experiments, considering a variability of ± 50 °C in the measurement related to the spatial distribution of heat and the position of the thermocouples. The exhaust temperature is similar, considering measurement uncertainty, between the natural gas and hydrogen combustion tests. The maximum furnace gas temperature was about 1150 °C.

Figure 3 – Comparison of key temperatures during the two melting tests.
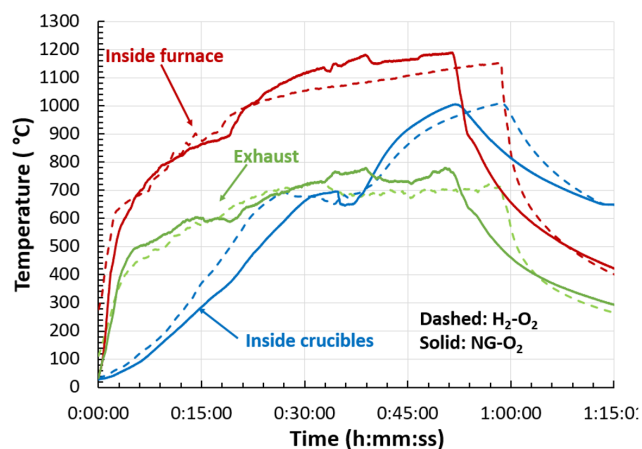
The crucible temperature shows the temperature increases first and then drops from about 700 °C to 670 °C at about 25–35 min after the start of the experiment. This is an indication of when aluminum melting begins and the thermocouple reading shows a change from measuring the gas temperature to the liquid melt temperature. The melted aluminum is further heated to 1000 °C before flame shut-down at 00:50 – 00:60. The furnace is then purged with nitrogen. The nitrogen purge helps to protect the molten metal and slag from further oxidation by oxygen (present in air) that could enter the furnace from outside. This allows the comparison of melts from different experiments in a consistent way.

The thermocouple inside the crucible indicates the aluminum charge heats up faster during the hydrogen-fired test as compared to the natural gas test. This is primarily driven by the flame characteristics as discussed in the results section and is not an indication that a hydrogen flame will heat the melt faster. The trend in an actual reverb furnace will depend on the flame type and burner design.

Post-experiment sample analysis:

The crucibles are removed from the furnace after the melt has solidified. A 0.5" thick slice is taken from this melt as shown in **Figure 4**. Test samples are collected from this slice (surface layer and core metallic layer). Three key features are investigated: the properties of the oxidized layer, the transition layer from oxide layer to metallic aluminum, and the core aluminum inside the melt.

XRD: An attempt was made to remove only the outer-most slag layer from the samples for XRD analysis. This was accomplished by using a vibratory tool across the outer surface. The surface was separated into a "right" and "left" side. The removed material from each side was collected and placed on a low background mount. The pieces were placed in an XRD mount and held in place using a portion of Leit-C Plast conductive putty. XRD data were collected from the mounted samples using a Panalytical X'Pert Pro MPD diffractometer with Co-Kα radiation and X'Celerator detector. Data were collected over the range 10° ≤ 2θ ≤ 115° using a 0.033° step size and a 500 sec/step count time. A 10 mm mask was used on the incident beam side to reduce the irradiated area on the samples.

SEM/EDS: For examination by SEM/EDS, the samples were prepared by mounting in a clear epoxy under vacuum. The mounted sample pieces were cross-sectioned using standard metallurgical polishing techniques. A layer of gold/palladium alloy was applied via sputter deposition. The mounted cross-sections were analyzed using a JEOL JSM-5910LV SEM operated at 15 kV accelerating voltage, coupled with a Thermo Noran System Six Si drifted EDS detector.

Figure 4 – The solidified aluminum piece (right) and the extracted samples for SEM-EDS analysis (left).
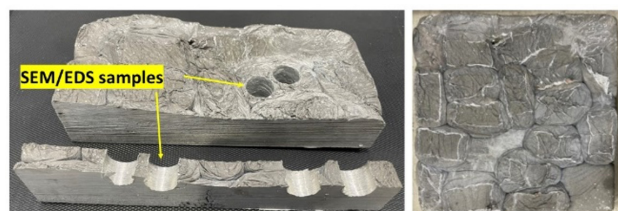
3.0 Results and Discussion

3.1 Flame

The oxy-natural gas and oxy-hydrogen flames are located about 12" above the crucibles. During the ramp-up to 0.4 MMBtu/hr, the hydrogen flame is shorter than the NG flame, resulting in a higher heat-release rate near the flame base and above the stainless-steel crucible on the right side of the furnace. This difference in heat release results in faster temperature rise inside the stainless steel crucible during the oxy-hydrogen melting test, as it was shown in **Figure 3**.

3.2 Dross formation

The mass of the aluminum charge in each crucible is measured post-melting, where a net gain in its mass is noticed due to oxidation. The results of weight measurements for the two aluminum loads are summarized in **Table 3** and show a relative increase of 0.14–0.28% in the initial mass of the samples. A similar net mass gain % was observed for the melt in the ceramic crucibles.

Table 3 – The aluminum mass measurements before and after the melting (*initial mass of alloy: 7.21 lbs).

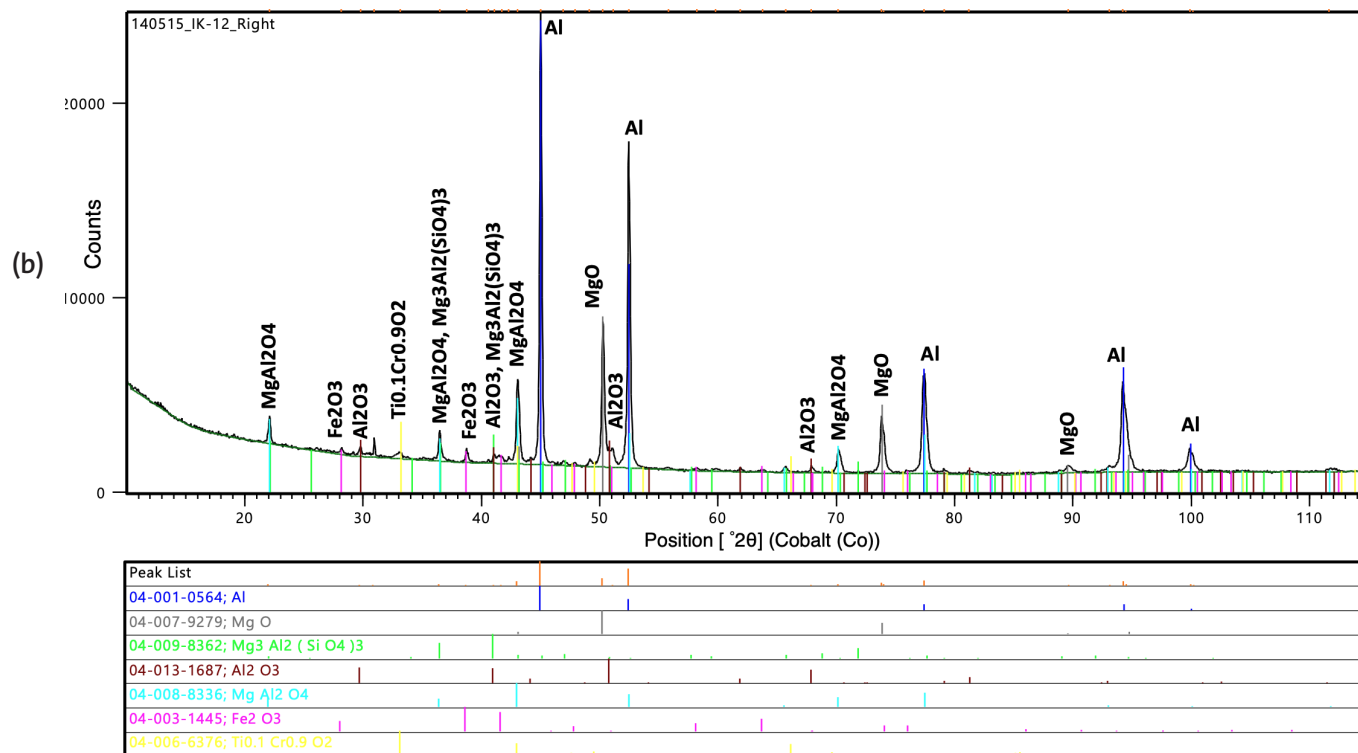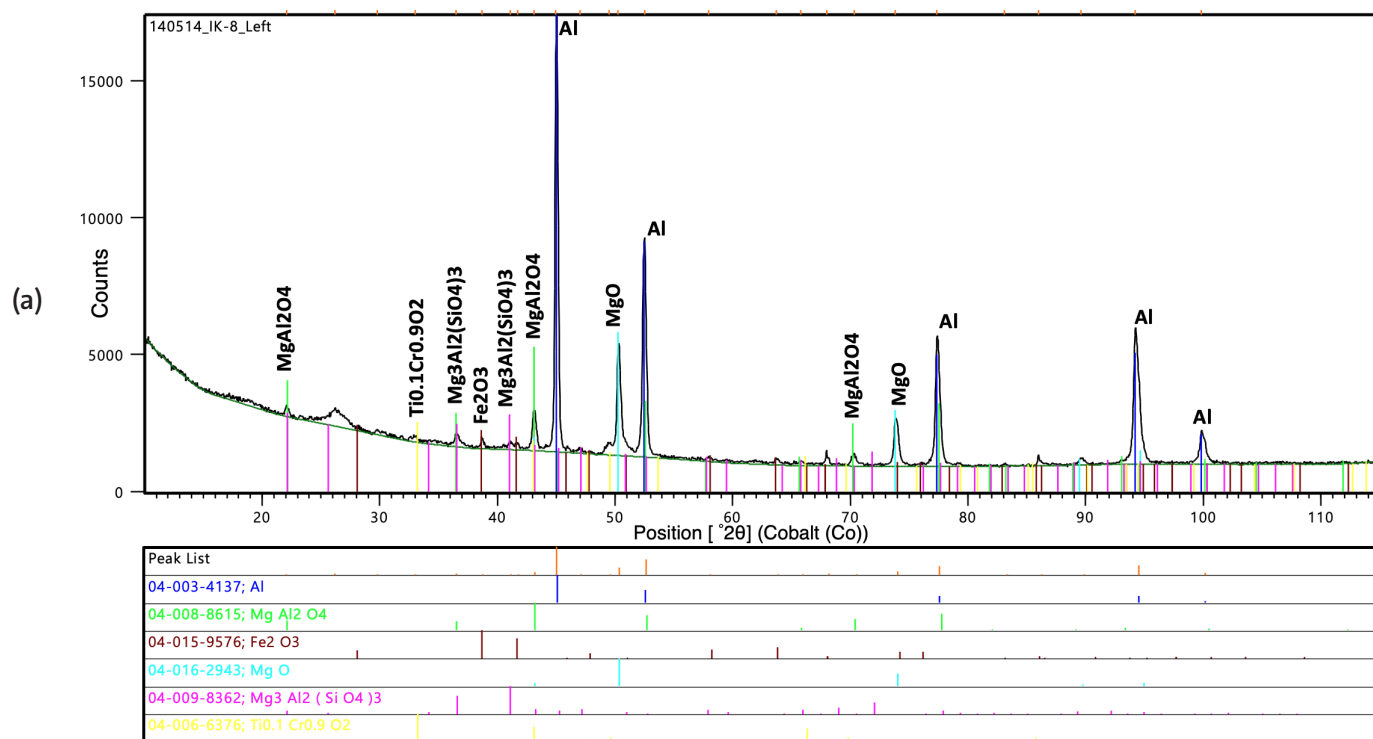|		NG - O_2	H_2- O_2
Mass of the loaded crucibles	Pre-melting	13.85 lb	13.64 lb
	Post-melting	13.87 lb	13.65 lb
Net mass gain (difference)	Absolute	0.02 lb	0.01 lb
	Relative*	0.28%	0.14%

Due to the preferential oxidation tendency of magnesium as compared to aluminum, the mass increase of the melt is strongly correlated to the concentration of magnesium in the MgAl alloy. The relative mass increase of the aluminum sample is in the range of the reported results in the literature of similar aluminum alloys with 0.8–1.2% magnesium content[3]. Considering the resolution of the measurement device (0.01 lb), the results indicate both NG and H_2 melted samples have similar mass gains due to oxidation.

3.3 Chemical composition analysis: slag/dross and melt

A powdered sample was collected from the oxidized dross layer of each melt (stainless steel crucible) as described in the previous section and placed in an XRD instrument for identification of crystalline phases. The samples were collected from melt regions located away from the crucible sidewall.

The results of the XRD analysis are shown in **Figure 5**, where the different crystalline phases are overlayed on the diffraction angle plot shown on the top for each sample. The aluminum phase present in the XRD spectrum corresponds to the metallic aluminum removed with the sample while collecting the slag powder. It was not possible to avoid the aluminum due to the thin oxide layer (~10 microns) as shown in the microscopy images in the next section.

Figure 5 – XRD analysis of powdered slag sample (a) NG-O₂ flame (b) H₂-O₂ flame

(a)

140514_IK-8_Left

Peak List
04-003-4137; Al
04-008-8615; Mg Al2 O4
04-015-9576; Fe2 O3
04-016-2943; Mg O
04-009-8362; Mg3 Al2 (Si O4)3
04-006-6376; Ti0.1 Cr0.9 O2

(b)

140515_IK-12_Right

Peak List
04-001-0564; Al
04-007-9279; Mg O
04-009-8362; Mg3 Al2 (Si O4)3
04-013-1687; Al2 O3
04-008-8336; Mg Al2 O4
04-003-1445; Fe2 O3
04-006-6376; Ti0.1 Cr0.9 O2

Besides the metallic aluminum, the two major phases present in XRD spectrum are the MgO (periclase) and $MgAl_2O_4$ (spinel) which correspond to the makeup of the oxide dross layer formed over the melt. The minor phases identified by the XRD analysis includes the silicate $Mg_3Al_2(SiO4)_3$, the iron oxide Fe_2O_3, and a titanium-chromium oxide $Ti_0.1Cr_{0.9}O_2$ phase, corresponding to minor elements present in the alloy. The makeup of the major compounds found in the oxide layer of the two samples is consistent with a previous study in the literatur[2].

The results, **Fig 5**(b), indicate the presence of alumina (Al_2O_3) in the sample melted with the oxy-hydrogen flame. Al_2O_3 was not detected in the slag sample from the NG-O_2 flame.

Comparison of XRD analysis of the melt core sample of NG-O_2 and H_2-O_2 is shown in **Table 4**. The five dominant peaks for both melts are aluminum and all other compounds/elements constitute very low counts. No Mg was detected, indicating Mg has preferentially segregated towards the melt surface. The results are from samples (10–12 mm) extracted from the core of the melt. It is possible the minor phases not detected in the samples are present in other parts of the melt.

Table 4 – Comparison of the melt sample (x: Detected in the sample, N/D: Not detected)

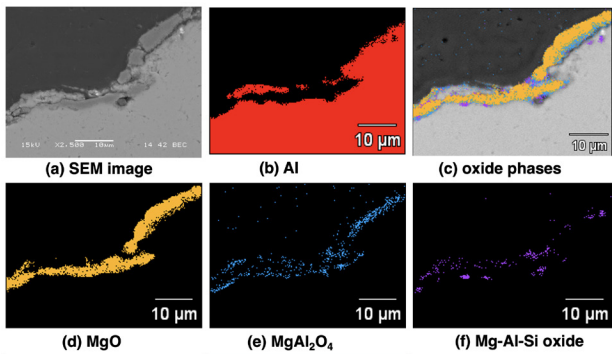|	Al	Mg_2Si	Al_2O_3	Si C	Fe0.5Al0.25	C	Fe Si	$TiCr_2$
NG-O_2	x	x	N/D	x	N/D	x	N/D	N/D
H_2-O_2	x	x	N/D	N/D	x	N/D	x	x

3.4 SEM/EDS analysis

The surface samples of the solidified melts from the two melting experiments were examined using an SEM/EDS to determine the morphology and the elemental composition of the dross oxide layer. EDS analysis is qualitative in nature and to quantify elemental concentrations, surface topology, homogeneity, etc. needs to be considered. EDS has been used to identify the major oxides (MgO and $MgAl_2O4$) that are formed from melting and the study[9] indicates that if Mg/O weight ratio is higher than 1, oxides contain a high percentage of pure MgO, and if the Mg/O ratio is less than 0.4 and Mg/Al ratio is about 0.44, oxides likely is $MgAl_2O_4$. In the current work, elemental composition from the SEM/EDS data, alongside the detected phases in the slag power XRD analysis, was used to map out the likely compounds present in the oxide layer on the SEM images as shown in **Figures 6–8**.

SEM/EDS images in **Figure 6** show metallic aluminum in the core covered by a layer containing different compounds/oxides on the sample surface exposed to the furnace atmosphere. The oxide consists of an MgO outer layer with $MgAl_2O_4$ present below the exposed surface. Other phases containing minor elements in the alloy are also present below this surface, such as a

silicon-containing phase as shown in the **Figure 6**(f). The presence of both MgO and $MgAl_2O_4$ indicates the breakaway oxidation (MgO formed in the first oxidation step reacting with Al to form $MgAl_2O_4$) has started, but the fact that MgO is still detected shows the breakaway oxidation has progressed partially.

Comparison of **Figures 6 and 7** shows the structure and composition of the exposed oxide layer formed on the melt from both the NG-O_2 and H_2-O_2 flames are similar and consistent with the pattern described above, an MgO-layer on the exposed surface with a more porous $MgAl_2O_4$ phase below the MgO layer. **Figure 7** shows formation of an internal oxidation zone, below the top oxide layer, that contains MgO, $MgAl_2O_4$, and Mg-Al-Si oxides. An aluminum layer separates the internal oxidation zone from the top oxide layer.

Figure 6 – SEM image and phases present in the dross layer of the sample melted with a NG-O$_2$ flame.

(a) SEM image

(b) Al

(c) oxide phases

(d) MgO

(e) MgAl$_2$O$_4$

(f) Mg-Al-Si oxide

Figure 7 – SEM image and phases present in the dross layer sample melted with a H$_2$-O$_2$ flame.

(a) SEM image

(b) Al

(c) Oxide phases

(d) MgO

(e) MgAl$_2$O$_4$

(f) Mg-Al-Si oxide

In some areas of the melt from the H$_2$-O$_2$ flame, SEM/EDS maps show a relatively uniform 3-4 μm MgO layer covering the inner phases and the core aluminum phase, as shown in Figure 8. Similar observations have been reported[2], where a sample from a high-moisture atmosphere (>69 vol.%) showed an MgO oxide layer formed on the exposed surface of the melt. This phenomenon could potentially protect the aluminum phase against further oxidation, reducing the melting losses.

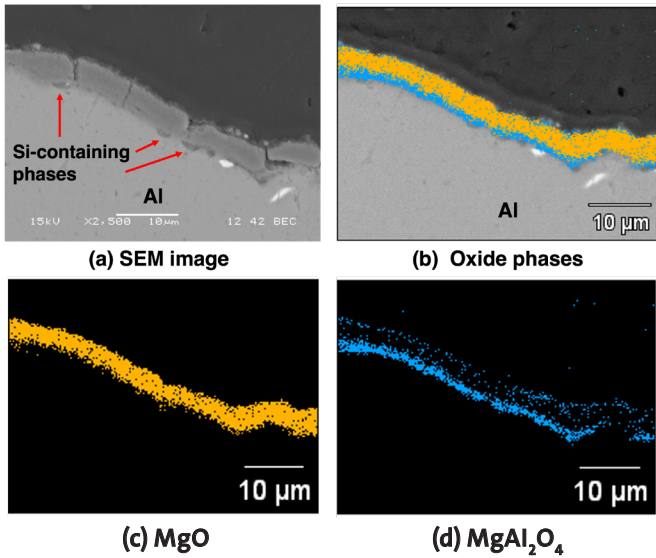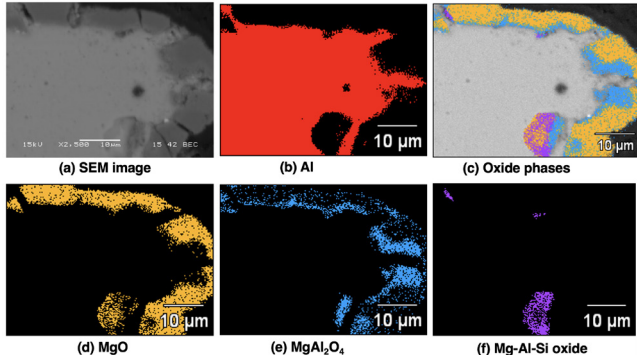**Fig 8: SEM image and major phases detected in the dross layer with SEM/EDS with H$_2$-O$_2$ flame.**

(a) SEM image

(b) Oxide phases

(c) MgO

(d) MgAl$_2$O$_4$

4.0 Conclusions

The impact of changes to the furnace atmosphere from using hydrogen versus natural gas fuel on the aluminum melting process and the melt properties was investigated in Air Products' Advanced Clean Energy Laboratory facilities. 6061 aluminum was melted in a test furnace equipped with a fuel-flexible oxy-fuel burner (either with 100% NG or 100% H_2 fuel). The furnace average temperature, crucible size and material load weight and shape, temperature-time history, and final melt temperature (1000 °C) were kept consistent for both experiments. Samples extracted from the solidified melt were analyzed using XRD and SEM/EDS.

Both melts (one using NG fuel and other using H_2) showed mass gains in the range of 0.14–0.28% of the initial charge which is in the expected range for aluminum alloys with low magnesium content (Mg ~0.8–1.2 wt.%). XRD patterns of dross/slag powder samples from the surface of the two melts indicated the presence of the two major oxides MgO (periclase) and $MgAl_2O_4$ (spinel) in the dross layer. SEM micrographs showed a dross layer with a thickness of a few microns formed on the exposed surface and an internal core consisting of aluminum. The dross layer consisted of an outermost MgO layer covering a more porous $MgAl_2O_4$ phase. Additionally, SEM micrographs from the sample melted with the oxy-hydrogen flame indicate formation of a more uniform MgO layer protecting the melt from additional oxidation.

The experimental results from this study are encouraging to consider oxy-hydrogen burners as a means to decarbonize secondary aluminum melting. The total mass gain (dross formed) and type of oxides formed is similar between hydrogen and natural gas fuels, demonstrating that melt yield was not adversely impacted with the fuel switch. Expanding the scope of future testing to include higher Mg-containing alloys and longer test runs will be needed for broader applicability across the secondary melting market. It is important to note that while the high moisture content in the furnace atmosphere with hydrogen fuel did not result in additional oxidation of the melt pool, proper selection of the refractory material will be needed under such conditions to avoid potentially detrimental effects on refractory life. However, these initial results provide a strong basis for scaled-up testing in a reverb furnace and the continued evaluation of hydrogen as a viable fuel for secondary aluminum melting operations.

References

1. Raabe, D., Ponge, D., Uggowitzer, P.J., Roscher, M., Paolantonio, M., Liu, C., Antrekowitsch, H., Kozeschnik, E., Seidmann, D., Gault, B. and De Geuser, F. (2022). Making sustainable aluminum by recycling scrap: The science of "dirty" alloys. Progress in Materials Science, 128: 100947.

2. Tichy S, Doppermann S, Pucher P, Prillhofer B, Wibner S, Antrekowitsch H (2024). Influence of water vapor on the oxidation behavior of molten aluminum magnesium alloys. In: Wagstaff, S. (eds) Light Metals 2024. TMS 2024. The Minerals, Metals & Materials Series, Springer, Cham.

3. Syvertsen, M., Johansson, A., Lodin, J., Bergin, A., Ommedal, M., Langsrud, Y., & Peterson, R. D. (2023). Oxidation Study of Al-Mg Alloys in Furnace Atmospheres Using Hydrogen and Methane as Fuel. In: Broek, S. (eds) Light Metals 2023. TMS 2023. The Minerals, Metals & Materials Series. Springer, Cham.

4. Piquard L, Clément E, Adendorff M, Iplik E, Ekman T (2024). Reverberatory Furnaces Decarbonization – The Case of Hydrogen Combustion: Proof of Concept and First Experimental Results on Borel Furnace. In: Wagstaff, S. (eds) Light Metals 2024. TMS 2024. The Minerals, Metals & Materials Series. Springer, Cham.

5. Sane A, Gangoli S, He X, Lawrence M, Hewertson R (2018). Effective Use of Oxy-Fuel Combustion in Aluminum Reverberatory Furnaces. Light Metal Age, August 2018, pp. 36-38.

6. Syvertsen M, Kvithyld A, Gundersen E, Johansen I, Engh TA (2019). Furnace Atmosphere and Dissolved Hydrogen in Aluminum. In: Chesonis C. (eds) Light Metals 2019. The Minerals, Metals & Materials Series. Springer, Cham.

7. Reddy BM, Nallusamy T (2021). Degassing of Aluminum Metals and Its Alloys in Non-ferrous Foundry. In: Kumaresan, G., Shanmugam, N.S., Dhinakaran, V. (eds) Advances in Materials Research. ICAMR 2019. Springer Proceedings in Materials, vol 5. Springer, Singapore.

8. Makwana A, He X, Hewertson R, Lawrence M (2022). Decarbonization of Secondary Aluminum Melting – Oxy-fuel Combustion and Low-Carbon Intensity Fuels. Light Metal Age, October 2022, pp. 32-37.

9. Wu G, Dash K, Galano ML, O'Reilly KAQ (2019). Oxidation studies of Al alloys: Part II Al-Mg alloy. Corrosion Science 155:97-108.

For more information, please contact us at:

Corporate Headquarters
Air Products and Chemicals, Inc.
1940 Air Products Boulevard
Allentown, PA 18106-5500
T 800-654-4567
info@airproducts.com

Canada
Air Products Canada Ltd
2233 Argentia Rd., Suite 203
Mississauga, ON L5N 2X7
T 800-654-4567/905-816-6670
info@airproducts.com

Europe
Air Products PLC
1000 Hillswood Drive
Chertsey
Surrey, KT16 0PS
UK
T +44(0)800 389 0202
apukinfo@airproducts.com

Asia
Air Products
Floor 2, Building #88
Lane 887, Zu Chongzhi Road
Zhangjiang Hi-Tech Park
Shanghai, 201203, P.R.C.
T +021-3896 2000
F +021-5080 5585
Sales hotline: 400-888-7662
infochn@airproducts.com

airproducts.com/nonferrous

AIR PRODUCTS

GENERATING A CLEANER FUTURE